Chapter 12

Zeta Potential and Colloid Reaction Kinetics

P. Mulvaney

12.1 Introduction

The solid–liquid interface has been the subject of experimental study for some 100 years, beginning with Gibbs, whose work on the thermodynamics of adsorption laid the foundations for interface science. The electrical aspects were investigated by von Helmholtz, Gouy, Chapman, and Stern, as well as other eminent scientists around the turn of the century. Their aim was to explain the structure of the interface and to understand how properties such as the electric potential and surface tension varied across the surface layers. In addition, early theories successfully explained the phenomenon of electrocapillarity, the origins of the Nernst or equilibrium electrode potential, and they could also predict, to within an order of magnitude, the electrical capacitance of an electrode immersed in water. However, it was always recognized that the structure of the electrical double layer (EDL) played an equally important role in electrode kinetics. Butler and Volmer subsequently determined how the kinetics of charge transfer depended on the electrode potential and demonstrated that the equilibrium electrode potential was directly related to the rate of electron transfer.

In the 1940s Derjaguin and Landau, and independently Verwey and Overbeek working in Holland, developed the basic theory of particle coagulation (the DLVO model) in terms of the electrical double layer around each colloid particle in solution [1]. They established that colloid coagulation is about the interaction of electrical double layers. A large body of evidence subsequently accumulated in support of the basic tenets of DLVO theory, and eventually, colloid chemistry adopted the entire electrical double layer structure and its associated thermodynamics as part of its foundations. However redox reactions at particle surfaces could not be readily investigated, and questions about kinetics at colloid surfaces – processes such as redox catalysis, colloid nucleation and dissolution, electron transfer by excited species generated in solution, and charge injection by photosensitizers – all remained largely unanswered. Such redox reactions are central to a plethora of important industrial processes ranging from the photographic process [2], the removal of rust [3], the decontamination of nuclear reactor coolant systems [4], the transport

of nutrients such as Mn^{2+} in natural waters [5], solar energy conversion [6], the degradation of paints, the removal of organic pollutants [7], and the electrochemical discharge of the alkaline battery [8]. Over the last 20 years, the use of optically transparent colloids together with the increased availability of stopped-flow spectroscopy, laser flash photolysis, and pulse radiolysis has finally enabled a direct comparison of colloid electrochemical kinetics with standard electrode kinetics to be made. In particular, whilst the equilibrium Nernst potential is fundamental to both areas of surface science, one can now assert that the Butler–Volmer equation (or Tafel equation in its simpler form) will soon be as important to colloid chemists as it is to the electrochemist.

In this chapter, we examine some of the available colloid data on the kinetics of electron transfer and try to highlight the parallels with conventional metal electrochemistry. We will focus on metal oxide particles because they are the most readily understood, and because the majority of the available experimental data have been gleaned from these materials. We begin by presenting a summary of the electrical structure of the metal-oxide–water interface. This enormous subject is covered in many texts in detail, particularly the underlying assumptions inherent in the derivation of the equations describing the double layer [9–13]. The aim here is to explain how the structure of the electrical double layer affects the actual rate of charge transfer at the particle interface. Such understanding will be fundamental to the improved design and exploitation of nanostructured materials [14, 15].

12.2 The EDL around Metal Oxides

12.2.1 The Helmholtz Region

When a conductor is placed into water, the steady state charge that builds up on the solid is usually due to charge transfer between the metal and solution. For example, a platinum electrode usually has an open circuit potential in aerated solution determined by the (largely irreversible) kinetics of the reaction [16]:

$$O_2 + H^+ + e^-(Pt) \rightarrow HO_2 \tag{12.1}$$

For semiconductors or insulators, the amount of charge that can be exchanged is much less, since the mobile charge is due only to impurities. As a consequence, it is usually the preferential loss of lattice cations and anions, or the adsorption of charged species from solution, that determines the amount of surface charge on a particle.

When a metal oxide surface is created in solution, the adsorption of hydroxyl ions or protons leads to the generation of a surface charge, and an electric potential develops between the surface and the bulk solution. Provided the surface activity of these so-called potential-determining ions (H^+, OH^-) remains constant, the surface potential of a metal oxide particle in aqueous solution is given by the familiar

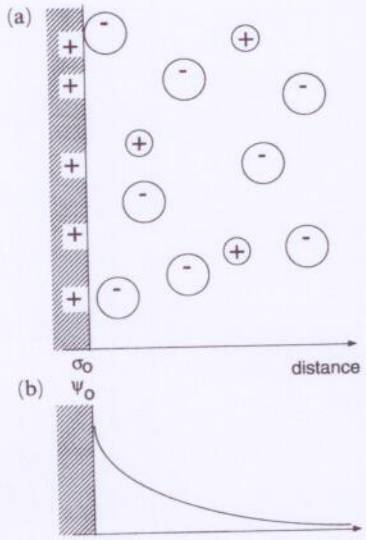

Figure 12.1. The diffuse layer. (a) The charge distribution near a charged surface, and (b) the potential distribution, which follows one of the four equations in Table 12.1.

Nernst equation:

$$\psi_0 = -0.059\ (\mathrm{pH} - \mathrm{pH_{pzc}}) \tag{12.2}$$

where $\mathrm{pH_{pzc}}$ refers to the pH at which there is equal adsorption of potential-determining cations and anions at the surface. In response to the adsorbed surface charge there will be a local excess of counterions around the particle. These counterions form a diffuse layer around the particle and cause the electric potential to slowly decay to zero as one moves away from the particle surface towards the bulk solution, as shown schematically in Figure 12.1. However, some of these ions may be strongly adsorbed, forming a plane of bound countercharge, which will lower the electric potential immediately adjacent to the particle surface. This region is usually called the Helmholtz or Stern layer and is made up of both strongly polarized water molecules and desolvated ions, as shown in Figure 12.2. The adsorption plane is located at a distance x_1 from the actual surface, and the relative permittivity in the region $0 < x < x_1$ is taken to be ε_1. ε_1 has a value usually taken to be between 2 and 6. Since the distance of these ions from the surface is only of the order of 3 Å, the surface and counter charge may be treated as a parallel plate condenser with a capacitance per unit surface area given by

$$K_1 = \sigma_0/(\psi_0 - \psi_1) = \varepsilon_1\varepsilon_0/x_1 \tag{12.3}$$

where $\varepsilon_1\varepsilon_0$ is the permittivity of the layer and σ_0 is the surface charge density. Consequently, the potential at x_1 is reduced to

$$\psi_1 = \psi_0 - \sigma_0/K_1 = \psi_0 - \sigma_0 x_1/\varepsilon_1\varepsilon_0 \tag{12.4}$$

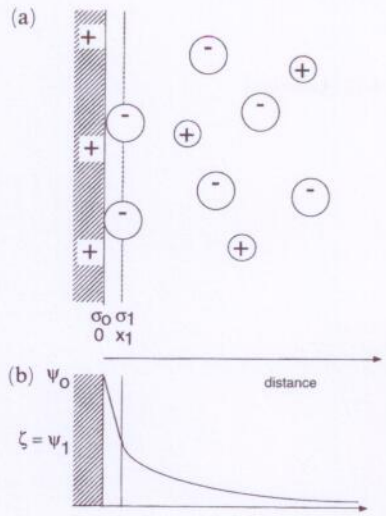

Figure 12.2. The electrical double layer with Stern or Helmholtz layer. (a) Charge distribution is broken up into a layer of specifically adsorbed ions and a diffuse layer. (b) The potential distribution showing the linear decay in the inner region and the diffuse layer potential, which begins at a distance x_1 from the surface and at a lower potential than ψ_0.

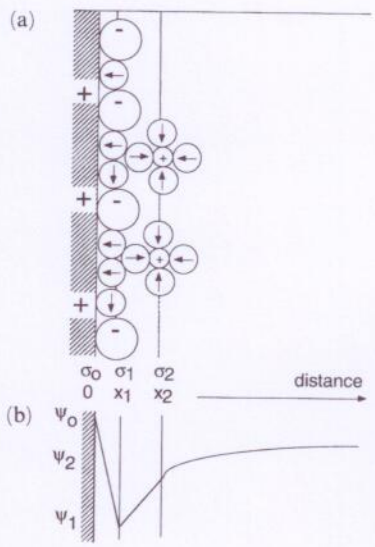

Figure 12.3. The electrical double layer according to the GCSG model. (a) Charge distribution includes an inner layer due to adsorbed ions and a second compact layer due to the finite size of hydrated ions approaching the surface from the diffuse layer. (b) The distribution of potential. For the case shown with superequivalent adsorption, the potential at x_1 or shear plane is the opposite to the intrinsic surface charge. There is also a linear variation in potential between x_1 and x_2.

It is important to realize that although ions adsorbed electrostatically at the Helmholtz plane will not completely neutralize the surface charge, if there is, in addition, a chemical driving energy for adsorption, the adsorbed countercharge may exceed that of the true surface charge, and the overall charge on the particle may be reversed. This is depicted in Figure 12.3 and we see that the potential actually changes sign, before decaying slowly to zero in bulk solution. This situation is often realised with polyelectrolytes such as poly(acrylic acid) or sodium hexameta-

phosphate, which can superadsorb on colloid surfaces. The ions in the Helmholtz layer are so strongly bound that an electric field applied to the colloid will cause motion of the particle, the adsorbed countercharge, and a monolayer or so of solvent molecules, i.e. the effective charge on the electrokinetic unit is not due solely to the surface charge, but will be reduced (generally) by the plane of countercharge.

In the GCSG (Gouy–Chapman–Stern–Grahame) model [17, 18] a second structural plane is also defined, and this is shown in Figure 12.3. This is at a distance x_2 and is the distance of closest approach of solvated ions to the plane x_1, owing to the finite size of the ion and its hydration shell. This second plane is usually termed the outer Helmholtz plane (OHP), with x_1 then being the inner Helmholtz plane (IHP). In this case, the electric potential decreases further between the inner plane of adsorbed anions and the OHP where counterions reach. It is the potential at x_2 which then orientates other ions in solution and induces the buildup of the space charge layer of counterions around the particle.

12.2.2 The Diffuse Layer

Electroneutrality requires that, overall, the excess charge density around the charged colloid particle in the diffuse layer, σ_d, must equal the charge density on the particle, i.e.

$$\sigma_o + \sigma_1 + \sigma_d = 0 \tag{12.5}$$

The electric potential at any point in the diffuse layer is calculated from Poisson's equation:

$$\nabla^2\psi = -\rho/\varepsilon_r\varepsilon_o \tag{12.6}$$

For a symmetrical $z{:}z$ electrolyte, the charge density at any point in solution is

$$\rho = \zeta e\,(n_+ - n_-) \tag{12.7}$$

where $|z|$ is the absolute electrolyte valency, and n_+ and n_- are the respective ion concentrations, at that point in the solution. Assuming the ions are distributed in the electric field according to the Boltzmann equation, then at any point we can write

$$n_\pm = n^\infty{}_\pm \exp\,(-z_\pm e\psi/kT) \tag{12.8}$$

where n^∞ is the bulk ion concentration, and combining Eqs. (12.8) and (12.9), we obtain the Poisson–Boltzmann (PB) equation:

$$\nabla^2\psi = -2n^\infty ze/\varepsilon_r\varepsilon_o \sinh\,(ze\psi/2kT) \tag{12.9}$$

The boundary conditions for integration are that in the bulk solution, the potential, and the electric field disappear:

$$\psi \to 0 \text{ as } x \to \infty \tag{12.10}$$

and

$$\mathrm{d}\psi/\mathrm{d}x \to 0 \text{ as } x \to \infty \tag{12.11}$$

whilst at the start of the diffuse layer, the potential must be ψ_1:

$$\psi_{(x=x_1)} = \psi_1 \tag{12.12}$$

The solution of the PB equation is not straightforward, and the method of solution can be simplified by considering four regimes in turn.

12.2.3 The Diffuse Layer for Micron-Sized Colloid Particles

If the particle radius is large, the double layer can be treated as flat, and Cartesian coordinates used. Further, if the diffuse layer potential at x_1 is small ($\psi \ll kT/ze$), then linearization of the exponential terms leads to

$$\nabla^2\psi = \mathrm{d}^2\psi/\mathrm{d}x^2 = \kappa^2\psi \tag{12.13}$$

where

$$\kappa^2 = 2n^\infty e^2 z^2/\varepsilon_r\varepsilon_o kT \tag{12.14}$$

is called the Debye–Hückel parameter or inverse double layer thickness. Eq. (12.13) can be directly integrated using the boundary conditions (Eq. 12.10, 12.11) to yield

$$\psi = \psi_1 \exp(-\kappa x) \tag{12.15}$$

This shows that a charged particle has an apparent surface potential ψ_1 which falls off to 1/e of its surface value over a distance κ^{-1} in an electrolyte solution. For high potentials, $\psi_1 > 25$ mV/z at 298 K, the linearization is no longer accurate, and Eq. (12.9) must be integrated. The result is

$$\tanh(ze\psi/4kT) = \tanh(ze\psi_1/4kT)\exp(-\kappa x) \tag{12.16}$$

These results for high and low potentials for large particles are summarized in Table 12.1. Eq. (12.16) reveals that even for high potentials the diffuse layer thickness is still κ^{-1}. We can see that the approximation of a flat double layer around a colloid particle will be valid if $\kappa a \ll 1$. To obtain the capacitance of the double layer we note that

Table 12.1. Solution to the PB equation for high and low surface potentials in a symmetric electrolyte for high and low surface curvature.

	Large Particles $\kappa a \gg 1$	Small Particles $\kappa a \ll 1$
low potentials < 25 mV	$\psi(x) = \psi_1 \exp(-\kappa x)$	$\psi(r) = \frac{a\psi_1}{r} \exp(-\kappa(r-a))$
high potentials > 25 mV	$\tanh(y/4) = \tanh(y_o/4) \exp(-\kappa x)$	$\nabla^2\psi = \frac{d^2\psi}{dr^2} + \frac{2}{r}\frac{d\psi}{dr} = \frac{2zn^\infty e}{\varepsilon_r\varepsilon_o} \sinh\left(\frac{e\psi}{kT}\right)$ (numerical solution only)
	where $y = \frac{ze\psi}{kT}$ and	$\kappa = \left[\frac{2z^2 e^2 n^\infty}{\varepsilon_r\varepsilon_o kT}\right]^{1/2}$

$$(\sigma_1 + \sigma_o) = -\varepsilon_r\varepsilon_o \, d\psi/dx_{|x=x1} \tag{12.17}$$

From (12.12),

$$d\psi/dx_{|x=x1} = -\kappa\psi_1, \tag{12.18}$$

and on substitution we get

$$K_d = (\sigma_o + \sigma_1)/\psi_1 = -\sigma_d/\psi_1 = \varepsilon_r\varepsilon_o\kappa. \tag{12.19}$$

Thus the diffuse layer around a particle with $\kappa a \ll 1$ behaves like a parallel-plate capacitor, with thickness κ^{-1}, which is why κ^{-1} is called "the diffuse layer thickness."

12.2.4 The Diffuse Layer for Nanosized Particles

Nanosized particles distinguish themselves from their conventional, and larger, micron-sized counterparts by the fact that the double layer must be considered spherical because, for colloid particles with diameters of 100 Å, the assumption of flat double layers is no longer accurate. For example, at 1 mM $NaNO_3$, the Debye length is 100 Å, so $\kappa a = 1$. Integration of Eq. (12.9) must now be carried out in spherical coordinates. For small potentials linearization of Eq. (12.9) yields

$$\psi(r) = \psi_1 a/r \exp(-\kappa(r-a)) \tag{12.20}$$

However, an electric potential of the same order as thermal energies is usually insufficient to prevent particle coalescence (see Section 12.2.5). So whilst the simplification renders the solutions more tractable, it does not provide accurate results for stable colloids with higher surface potentials, and the use of the linearized forms is generally inadequate. For highly charged particles, the potential distribution must

be solved numerically through, for example, Runge–Kutta methods (see Section 12.2.5 below for an analytic approximation). The presence of the diffuse layer around an electrostatically stabilized colloid particle is essential. It is the repulsion experienced by two colloid particles as their double layers overlap that stabilizes them against coagulation. A high diffuse layer potential and a low electrolyte concentration, which increases the range of repulsion, are necessary for good colloidal stability. (In saying this, we ignore the possibility that the particles may be stabilized by polymers or large surfactants.)

We can now write down the total potential distribution between the particle surface and solution for an insulating or semiconducting metal oxide particle immersed in aqueous solution. For the model shown in Figure 12.2, we have

$$\psi(x_1) = \psi_o - \sigma_o/K_1 \tag{12.21}$$

$$\psi(x > x_1) = f(\kappa, a, \psi_1) \tag{12.22}$$

$$\psi_o = -0.059\ (pH - pH_{pzc}) \tag{12.23}$$

Here, $f(\kappa, a, \psi_1)$ refers to one of the four solutions in Table 12.1. Clearly, even for a model with just a single inner region, there are a number of experimental variables which need to be measured in order to quantify the potential distribution. Given that ε_1 and x_1 are not really directly accessible to experimental verification, simplifications are often advisable. Furthermore, until now, most electrokinetic investigations of colloid systems have been confined to the situation where only indifferent ions such as Na^+ or NO_3^-, are present in solution. In order to carry out electron transfer studies, there must be a redox couple present as well. Further simplification arises if the chemistry in solution can be controlled. By assuming there is no specific adsorption from solution we can set $\sigma_1 = 0$. However, this is clearly a poor approximation if a polyelectrolyte or surfactant has been used to stabilize the particles, or if a strongly chemisorbed ligand such as a thiol or amine derivative has been used to minimize particle growth during preparation. There has been little work done on the specific adsorption of redox couples, or even with simple carboxylic acids such as sodium citrate, which are extensively used to stabilize nanosized metal colloids.

12.2.5 The ZOS Model for Poorly Defined Nanoparticles

Before we discuss the process of electron transfer at colloid surfaces, we will present a simplified analytic version of the standard Stern model shown in Figure 12.2, which will allow us to understand the basic electrochemical kinetics involved, without needing to specify all the parameters of a complete double layer model. The double layer is broken up into a single Helmholtz layer of thickness x_1 and dielectric constant $\varepsilon_1\varepsilon_o$, i.e. with a constant capacitance given by

$$K_I = \varepsilon_1\varepsilon_o/x_1 \tag{12.24}$$

There is no specific adsorption at the plane x_1, which is also taken to be the start of the diffuse layer, i.e.

$$\sigma_1 = 0, \tag{12.25}$$

and

$$\sigma_o = -\sigma_d. \tag{12.26}$$

Finally, to link the electrical double-layer potentials to experimentally accessible data, we assume that the potential at x_1 is identical to the observed, measured "zeta potential."

$$\psi_1 = \zeta. \tag{12.27}$$

For particles in the size regime 30–100 Å, the condition $x_1 \ll a$ still holds and the flat-plate condenser model for the inner layer is justified. However, the diffuse layer thickness, characterised by the Debye–Hückel parameter κ^{-1}, is now much larger than a. The diffuse layer must be considered spherical. In principle, we need to solve the PB equation numerically, but we can save ourselves computational effort by adopting one of the various analytic approximations to Eq. (12.9) that have been developed. Ohshima et al. [19] found that for a sphere of radius a immersed in a 1:1 electrolyte of Debye–Hückel length κ^{-1}

$$\frac{\sigma_d e}{\varepsilon\varepsilon_o \kappa kT} = 2\sinh\left(\frac{e\zeta}{2kT}\right)\left[1 + \frac{2}{A\cosh^2\left(\frac{e\zeta}{kT}\right)} + \frac{8\ln\left[\cosh\left(\frac{e\zeta}{4kT}\right)\right]}{A^2\sinh^2\left(\frac{e\zeta}{2kT}\right)}\right]^{1/2} \tag{12.28}$$

where $A = \kappa a$. The diffuse layer charge, zeta potential, and surface potential are linked by

$$\zeta = \psi_1 = \psi_o - \sigma_o/K_I = \psi_o + \sigma_d/K_I. \tag{12.29}$$

We can now describe the double-layer structure using just one or two parameters, provided we have zeta potential data, which includes the point of zero charge (pH_{pzc}). ψ_o is deduced directly from the pH of the experiment (through Eq. (12.2)). Then from Eq. (12.28), we obtain σ_d using ζ, and a. From Eq. (12.29), this gives us K_I directly. The validity of this approach can be tested using zeta potential data over a wide pH range to determine the average value of the Helmholtz capacitance. This is shown in Figure 12.4, where κa has been fixed at 1 and zeta potential vs. pH data have then been generated for various values of K_I. If no zeta potential data are available for a particular system, then as a last resort, we can use values of K_I determined for micron sized particles of the same material via electrophoresis, and try to create artificial zeta potential vs. pH curves. This model contains the funda-

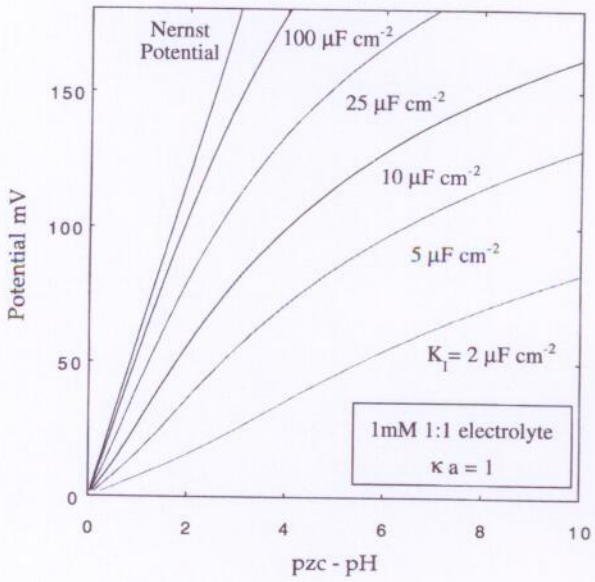

Figure 12.4. The calculated values of ζ vs. pH for nanosized colloid particles with $a = 100$ Å and 1 mM 1:1 electrolyte (i.e. $a = 1$) for different values of the inner layer capacitance, K_I. The diffuse layer charge is calculated from Eq. (12.28), and then ζ is obtained from Eqs. (12.2, 12.29).

mental features required to explain both colloid stability and redox chemistry at a nanoparticle surface. There is a diffuse layer, whose thickness depends upon the electrolyte concentration and surface potential, and an inner layer, the potential across which is controlled via the pH and inner layer capacitance. Because it contains no Stern layer charge and analytical approximations are used for the solution of the PB equation, this model is called the zero order Stern model (ZOS). The way the electric double layer potential is partitioned between the Helmholtz and diffuse layers critically determines both colloid stability and electron transfer kinetics.

12.2.6 The Point of Zero Charge and the Isoelectric Point

All these various double layer models have been designed by colloid chemists to explain the structure of the electrical double layer. In particular, they explain the apparent surface charge density obtained when a suspension is titrated with acid and base, and the observed mobility of the suspension particles when subjected to an electric field at different pH values. Because of the possibility of specific adsorption to colloid particles, there are two possible reference points for the measurement of the electric potential during mobility studies. These are the point of zero charge (pzc) and the isoelectric point (iep) of the solid [13]. The pzc is defined as the concentration of potential determining ions for which the surface charge σ_o is zero. For metal oxides, this corresponds to the pH at which $\Gamma_{H^+} = \Gamma_{OH^-}$, where Γ signifies the adsorption density. The isoelectric point is the concentration of potential determining ions at which the zeta potential is zero. They are often used interchangeably, but this is only the case if, at the pzc, there is no charge at the IHP. Thus, at the i.e.p. $\sigma_o = \sigma_1$ and therefore $\sigma_d = 0$. Conversely, at the p.z.c. $\sigma_o = 0$, and $\sigma_1 = -\sigma_d$.

12.3 Colloid Electron Transfer Kinetics – Theory

We now consider how the kinetics of electron transfer to particles are affected by this electrical double layer structure postulated to explain observed electrokinetic data. The two equations necessary are Fuchs' equation, (also used to describe the kinetics of colloid coagulation,) and the Tafel equation which quantifies the electric field dependence of the electron transfer rate constant.

12.3.1 Mass-Transfer-Limited Reactions

The rate constant for the steady state, diffusion-controlled reaction in solution between two species is given by the familiar Smoluchowski expression,

$$k_{\text{diff}} = 4\pi RD, \tag{12.30}$$

where $R = R_{\text{coll}} + R_{\text{rad}} \sim R_{\text{coll}}$ is the combined reaction radii of the electroactive species and the colloid particle, and $D = D_{\text{coll}} + D_{\text{rad}} \sim D_{\text{rad}}$, the combined diffusion coefficient. However charged species will also experience a force due to the electric field around the particle at any pH other than the pzc. The flux of an ionic species with concentration c and charge z_{R} towards a spherical surface in the presence of a position dependent electric field $\psi(r)$ is [20]

$$J = -D\left[\frac{\mathrm{d}c}{\mathrm{d}r} + c\frac{z_{\text{R}}e}{kT}\frac{\mathrm{d}\psi}{\mathrm{d}r}\right] \tag{12.31}$$

The boundary conditions are that $c = 0$ at $r = a$ and $c = c^{\infty}$ (the bulk radical concentration) at $r = \infty$. Integration yields

$$k_{\text{field}} = \frac{4\pi D}{\int_a^{\infty} \exp\left(\frac{z_{\text{R}}e\psi(r)}{kT}\right) r^{-2}\,\mathrm{d}r} \tag{12.32}$$

The integral in the denominator is the reciprocal of the effective reaction radius. When $\psi(r) = 0$, Eq. (12.32) reduces to the Smoluchowski equation; in the presence of a nonzero field, the denominator can be greater than or less than a^{-1}, depending on the signs of z_{R} and $\psi(r)$. Note that even in the presence of a field, steady state conditions prevail after $\sim 10^{-7}$s, so that the time dependence of the flux can be ignored in almost all colloid systems unless the suspension is very concentrated. e.g. for TiO_2 colloids with a = 50Å, the half-life for reaction with $(CH_3)_2COH$ ($k = 5 \times 10^{10}\,M^{-1}s^{-1}$, [21]) is 10ns only at 0.5 M TiO_2. It is unusual to work at such concentrations because of particle coalescence or because of the extremely high absorbance of such sols, which renders time-resolved work by spectroscopic means quite difficult.

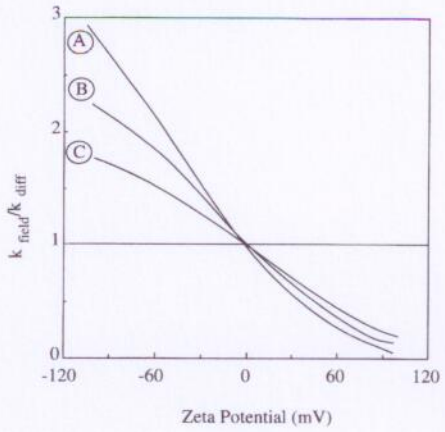

Figure 12.5. The effect of particle zeta potential on the mass transfer limited rate constant for radicals with charge +1 and particle radius 20Å. The ionic strengths are (a) 100 mM, (b) 10 mM and (c) 1 mM. The rate at the pzc is the Smoluchowski limit. Adapted from ref. 23.

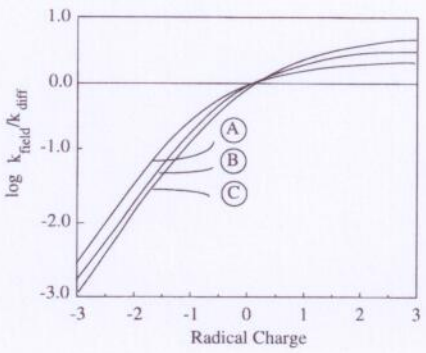

Figure 12.6. The effect of the radical charge on the mass transfer limited rate constant for a zeta potential of −80 mV and for ionic strengths (a) 1 mM, (b) 10 mM and (c) 100 mM assuming a particle radius of 20Å. The rate at z = 0 is the Smoluchowski limit. Curve is drawn through nonintegral values of charge for ease of comparison. Adapted from ref. 23.

Solution phase reactants can only approach the surface to the distance x_1 [18, 22]. Hence, the metal oxide can be considered to have a radius a and surface potential ζ, so that the boundary condition required for the integration of Eq. (12.29) is $\psi(a) = \zeta$. Once at the shear plane, transfer or deactivation occurs instantly. Thus for mass transfer limited reactions, we need to know D_{rad} and a, to calculate the Smoluchowski limit. In addition, when there is significant migration we need n^{∞} (the bulk electrolyte concentration), z_R (the radical charge) and ζ.

To see how the field affects the mass transfer limited rate constant, calculated values are shown in Figures 12.5 and 12.6 for conditions typical for nanosized colloids in aqueous solution. Figure 12.5 illustrates the dependence on the ζ potential (for $z_R = 1$) for three different electrolyte concentrations and Figure 12.6 the dependence of the mass transfer limited rate constant on the radical charge (at $\zeta = -80$ mV). A particle radius of 20Å was assumed in calculating the potential profile. In each case, the potential distribution was first calculated from the nonlinear PB equation using the given parameters a, κ, ζ. (2000 points out to a distance of $10\kappa^{-1}$). Then for a given value of ζ, and the radical charge, the flux at the surface

was calculated by a second integration using Eq. (12.32). As is clear from the results, diffusion controlled radical-colloid interactions are strongly dependent on the double layer properties (salt concentration, ζ, particle radius) and the magnitude of the radical charge. The flux of charged species due to migration rivals that due to the concentration gradient at high potentials and low ionic strength. When the two supplement each other, the rate may triple or quadruple, even at low radical charge. This should be readily discernible using flash photolysis or pulse radiolysis techniques. When the effects of the fluxes are opposing, the effect is far more dramatic, and the net flux to the colloid particle may be retarded by several orders of magnitude. Consequently, the effect of the zeta potential on mass transfer will be most clearly seen when the double layer acts to retard diffusion. In some cases a second order rate constant of just 10^7 M^{-1} s^{-1} may correspond to the mass transfer limit. Given that low ionic strength and high zeta potentials are usually necessary for ionically stabilized sols, the usual criterion that the diffusion limit is reached at a value of $\sim 10^{10}$ M^{-1} s^{-1} will no longer be valid.

Increases in salt concentration will decrease the importance of the migration term for mass transfer limited reactions. The effects of added indifferent electrolyte will be to decrease ζ and to compress the double layer simultaneously. (Since the diffuse layer capacitance is increased, there is a larger potential difference across the Helmholtz region.) However as can be seen from the figure, even in 0.1 M 1:1 electrolyte, pronounced deviations from the Smoluchowski value would be expected.

12.3.2 Activation-Controlled Electron Transfer

For electron transfer into a colloid particle, by a solution species (anodic reactions), the Tafel equation for the anodic electron transfer rate constant k_{et} is given by

$$\log \frac{k_{et}}{k_{et}^{pzc}} = \frac{\beta F \Delta\psi}{2.303RT} \tag{12.33}$$

where $\Delta\psi$ is the electric potential difference between the particle surface and the plane of electron transfer, and k_{et}^{pzc} is the rate constant at $\Delta\psi = 0$. If the ionic strength is high, the diffuse layer capacitance $K_d \to \infty$, and the total double layer field is confined to the Helmholtz layer. The zeta potential then approaches zero. Under these conditions, the entire change in electrode potential can be considered to act on the electrons tunnelling from donor to surface (or surface to donor). However in colloid systems, a high salt concentration will destabilize the sol, since if $\zeta \to 0$, there is no resistance to coagulation. At low ionic strength, the changes in surface potential will not just appear as an overpotential for electron transfer. Some of the electric potential is "lost" in the diffuse layer. The amount "lost" will depend on the relative capacitances of the two layers of the electric double layer. However, the diffuse layer potential governs the local concentration of electroactive ions. Thus, the pH dependence of the rate of electron transfer depends on the zeta potential in two ways. The potential difference $(\psi_o - \zeta)$ alters the rate constant for

electron transfer through Eq. (12.33), while the change in ζ potential alters the local concentration of any charged reactants through the Boltzmann equation, Eq. (12.8). When both are included, Eq. (12.33) assumes the form [24, 25]:

$$\log \frac{k_{et}}{k_{et}^{pzc}} = -\beta(\text{pH} - \text{pzc}) - \frac{(\beta + z_R)F\zeta}{2.3RT} \tag{12.34}$$

where is the transfer coefficient for the anodic electron transfer to the colloid and z_R the charge on the reductant. This equation is only valid for simple anodic electron transfer from the OHP. For cathodic electron transfer to an oxidant with charge z_O, the dependence on zeta potential is given by

$$\log(k_{et}/k_{et}{}^{pzc}) = (1 - \beta)(\text{pH} - \text{pH}_{pzc}) - (z_O + \beta - 1)F\zeta/2.303RT \tag{12.35}$$

The conduction band energy level in the colloid particle is normally the acceptor level for the transferred electron, and at the pzc, this energy level will not be identical to the redox potential of the solution couple. To compare intrinsic rates of electron transfer for the same solution couple with various colloidal semiconductors, it is necessary to decouple this chemical free energy term, $\Delta E_{pzc} = E^{cb}{}_{pzc} - E_{redox}$, which drives the reactions at the pzc. Thus the most useful parameter is $k_{et}{}^{ref}$ given by:

$$k_{et}{}^{ref} = k_{et}{}^{pzc} \exp(-F\Delta E_{pzc}/RT) \tag{12.36}$$

where for convenience we assume that the energy levels are potentials on a suitable electrochemical scale.

12.3.3 The Transition between Activation and Mass Transfer Limits

The transition between diffusion and activation control has been discussed by several authors for the case of zero migration [26,27]. The observed rate constant can be readily derived by consideration of the steady state concentration of a reductant at the electron transfer plane to a single colloid particle. Let this be denoted c_{OHP}. The flux due to surface reaction is then $4\pi a^2 k_{et} c_{OHP}$, where k_{et} is the rate constant for electron transfer. This must be balanced by the flux from solution. Integrating Fick's Law with the boundary condition that $c = c_{OHP}$ at $r = a$ rather than $c = 0$ yields

$$k_{obs}\, c^{\infty} = 4\pi a D(c^{\infty} - c_{OHP}) = 4\pi a^2\, k_{et}\, c_{OHP} \tag{12.37}$$

It can be seen from this equation that the maximum flux to the OHP occurs if $c_{OHP} = 0$, which occurs as k_{et} increases. Conversely, the concentration gradient reduces to zero if $k_{et} = 0$, as expected intuitively. After rearrangement, the observed bimolecular rate per particle is

$$\frac{1}{k_{obs}} = \frac{1}{4\pi a^2}\left[\frac{1}{k_{et}} + \frac{a}{D}\right] \tag{12.38}$$

The same manipulations can be used when there is an electric field present around the particle, and in this case the transition from activation control to mass transfer control obeys

$$\frac{1}{k_{obs}} = \frac{1}{4\pi a^2}\left[\frac{1}{k_{et}} + \frac{a^2}{D}\int_a^\infty \exp\left(\frac{z_R e\psi(r)}{kT}\right) r^{-2}\,dr\right] \tag{12.39}$$

Clearly, the mass transfer rate constant depends on pH for charged reactants. So, for a reaction which is diffusion controlled over a wide pH range, as might be expected for many colloid reactions with e^-(aq) for example, a pH dependent reaction rate will be found.

12.4 Colloid Kinetics – Experimental Data

12.4.1 The Effect of pH

Various research groups have examined the rate of disappearance of a solution species via electron transfer to colloid particles, or conversely the transfer of electrons to acceptors in solution following photoexcitation of a semiconductor colloid. We cite the studies by Grätzel with TiO_2 [26–28], Darwent and coworkers [29–31], Willner [32] on silica, Bahnemann et al. on ZnO and TiO_2 [33], and Swayambunathan et al. on iron oxide [24, 25]. For many systems the chosen reactants have been radiolytically or photolytically generated, and the rate constants have been found to be close to the mass transfer limit.

Grätzel and Frank initially reported the very dramatic effect of pH on the rate constant for electron transfer using colloidal TiO_2 and methyl viologen as electron acceptor. Their results shown in Figure 12.7, clearly revealed the exponential de-

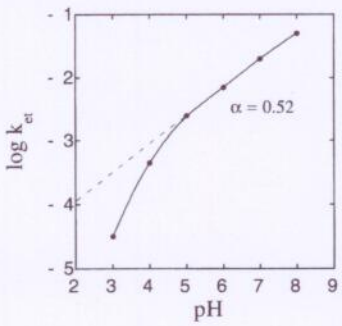

Figure 12.7. The relative rates of electron transfer from photoexcited colloidal TiO_2 to methyl viologen dications as a function of pH. Adapted from ref. 26.

pendence on pH predicted by classical electrochemical kinetics. This work was the first to show that even when the Helmholtz potential difference is governed by ion adsorption from solution and not by the electrical charge provided through an external power supply, the Tafel equation is still applicable. The ionic strength is not mentioned in their paper so it is difficult to reliably assess the importance of diffuse layer corrections [26].

12.4.2 The Effect of Electrolyte Concentration on Electron Transfer

Darwent et al. examined for the first time the role of diffuse layer contributions to the kinetics of electron transfer. They demonstrated that all electron transfer rates depend on ionic strength except at the pzc, as shown in Figure 12.8. They corrected their data for the diffuse layer contribution, using Debye–Hückel theory, modelling the nanosized titania colloids as large charged molecules. By employing weak double layer theory, i.e. low potentials, they showed that the observed transfer coefficient for metal oxide colloids obeys

$$\alpha \sim \alpha_o + (B + C\,I^{0.5})^{-1} \tag{12.40}$$

where I is the ionic strength and B and C are adjustable parameters. This equation is similar to the one employed in metal electrode kinetics at low overpotentials. The parameters B and C are related to the relative capacitances of the diffuse and Helmholtz layers, and α_o is the transfer coefficient at infinite ionic strength. In Figure 12.9, we have attempted to reanalyse their results using electrophoretic data gleaned from the work of Wiese and Healy [34]. Good agreement is obtained, both for different pH values and for large variations in ionic strength using Eq. (12.35). This clearly illustrates that instead of using B and C as adjustable parameters, experimental zeta potentials can be used to quantify the effects of ionic strength on the rates of electron transfer.

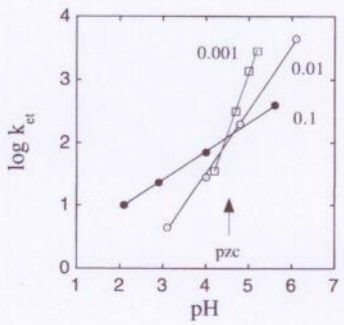

Figure 12.8. The effect of ionic strength and pH on the rate of electron transfer from colloidal TiO_2 to methyl viologen dication in the region around the pzc. Adapted from ref. 29.

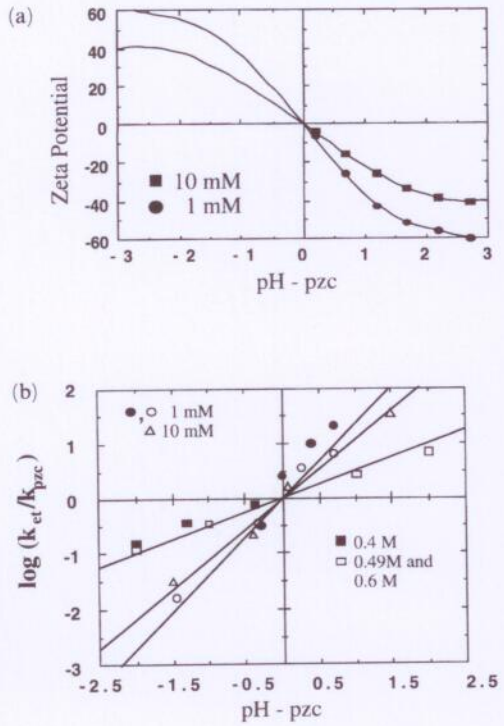

Figure 12.9. (a) Zeta potentials for TiO_2 at 1 mM and 10 mM vs pH from Wiese and Healy [34]. (b) Fits to the data of Darwent et al. using the zeta potential data from Wiese and Healy and Eq. (12.35). Adapted from ref. 25.

12.4.3 The Effect of the Zeta Potential and Radical Charge on the Rate of Electron Transfer

The only electron transfer experiments to date in which zeta potentials have been measured directly on the same nanosized particles is in the work of Swayambunathan et al. [24, 25]. Their results for electron transfer to colloidal iron oxide from both anionic and cationic viologen radicals are shown in Figure 12.10. By using two viologen radicals with opposite charge but virtually identical redox potentials, they confirmed that electrostatic effects dominate the kinetics of e.t. in solution. The rate of electron transfer for both radicals coincides at the pzc, again highlighting the fact that the pzc is the natural reference point for measuring transfer kinetics. However, rather than resorting to Debye–Hückel theory, valid only at low surface potentials, Swayambunathan et al. measured the zeta potential as a function of pH. The reaction becomes mass transfer limited for the anionic viologen radical at low pH as the surface potential of the iron oxide particles becomes very positive. Consequently, the kinetics must include both activation and mass transfer equations.

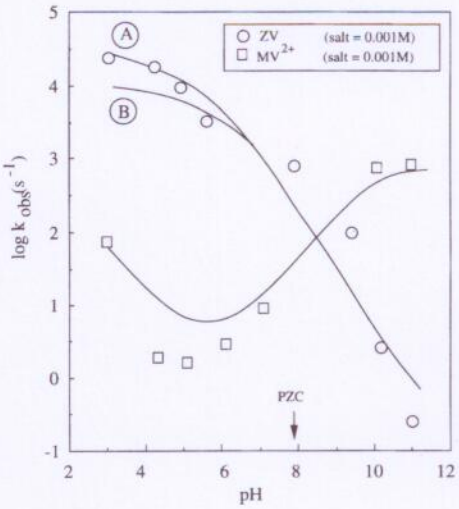

Figure 12.10. The effect of pH on the rate of electron transfer to colloidal ferric oxide particles from cationic and anionic viologen radicals. At low pH, the rate becomes mass transfer limited for the anionic viologen radical. Ionic strength = 1 mM. Particle radius = 20Å. Fits using Eqs. (12.34, 12.38 and 12.39).

$$\frac{1}{k_{\text{obs}}} = \frac{1}{4\pi a^2}\left[\frac{1}{k_{\text{et}}^{\text{pzc}} \exp\left(-\beta(\text{pH} - \text{pzc}) - \dfrac{(\beta + z_{\text{R}})e\zeta}{2.303kT}\right)} + \frac{a^2}{D}\int_a^{\infty} \exp\left(\frac{z_{\text{R}} e\psi(r)}{kT}\right) r^{-2}\,\mathrm{d}r\right] \tag{12.41}$$

In Figure 12.10, two curves are shown. One of these (curve B) uses the conventional Smoluchowski equation for the calculation of the mass transfer limit, based on Eq. (12.38), together with Eq. (12.34) for k_{et}. From the discussion above, the double layer corrected form, Eq. (12.39), should be better, since the radicals are charged and migration will contribute to the mass transfer of the radical to the colloid surface. Curve A uses Eq. (12.41) which is derived from Eq. (12.39) and Eq. (12.34). However the reaction only becomes mass transfer limited at low pH's, and below pH 3, the increasing solubility of the oxide and increasing electrolyte concentration make comparison with the theoretical values more difficult. The mass transfer limit in this pH range was calculated from Eq. (12.39), using the radius $a = 20$Å, as established by electron microscopy. The inclusion of the migration term does appear to give a better fit to the data than Eq. (12.38) over the limited pH range in which the reaction is diffusion controlled. The observed rate corresponds to a second order rate constant about twice that predicted by the Smoluchowski equation. It is worth noting that the transition to diffusion-migration control takes place over quite a wide pH range, and extends to pH 7, where the reaction is well below the expected mass transfer imposed limit.

It is clear that the entire pH dependence of the rate constants can be unified through the assumption that the zeta potential is close to the potential at the plane of electron transfer. In fact if the zeta potentials were about 10–20 mV higher, the

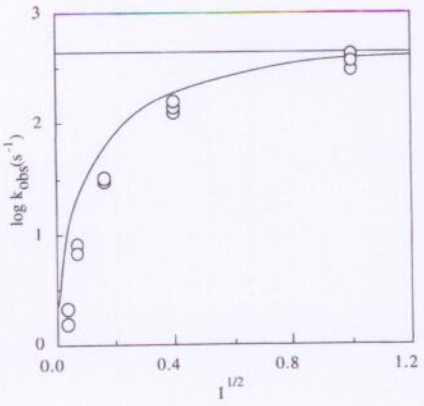

Figure 12.11. The effect of increased ionic strength on the rate of electron transfer to colloidal iron oxide from cationic methyl viologen radicals at pH 5.5. Fit to Eq. (12.34) with $\alpha = 0.5$, using $a = 20$Å, pzc $= 8.1 \pm 0.3$ using complete solution to the nonlinear PB equation and a Stern layer with $K_I = 400\ \mu Fcm^{-2}$. Adapted from ref. 24.

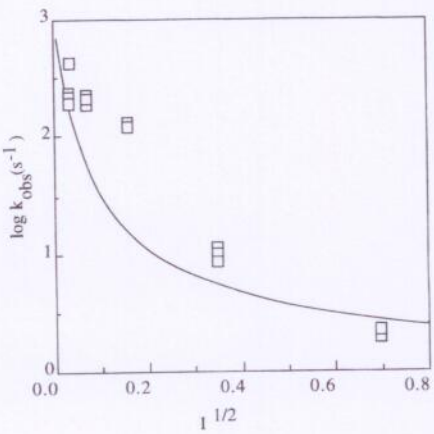

Figure 12.12. The effect of increased ionic strength on the rate of electron transfer to colloidal iron oxide from cationic methyl viologen radicals at pH 11. Fit to Eq. (12.34) with $\alpha = 0.5$, using $a = 20$Å, pzc $= 8.1 \pm 0.3$ using complete solution to PB equation and a Stern layer with $K_I = 400\ \mu Fcm^{-2}$. Adapted from ref. 24.

agreement would be almost perfect, an indication perhaps that the shear plane lies just beyond the true plane of transfer. Swayambunathan et al. also studied the role of electrolyte concentration [25]. As can be seen in Figure 12.11, the rate at pH 5.5 increases dramatically as salt is added, because of decreased repulsion between the positively charged radical and the positively charged colloid particles. The rate is 400 times faster in 1M electrolyte ($NaClO_4$) at pH 5.5. Conversely, above the pzc, the rate of transfer decreases as the attraction between the now negatively charged sol and the radical is reduced (see Figure 12.12). Unlike the case in purely ionic systems the plot of log k_{obs} versus $I^{1/2}$ is not linear. By extrapolating the rate constant to infinite ionic strength, an estimate can be made of the rate of electron transfer (at pH 5.5 and pH 11.0) when the electric potential is entirely confined to the Helmholtz layer, and all pH changes act as an overpotential for the charge transfer. These data are plotted in Figure 12.13. The rate constants at infinite ionic strength represent the case of electron transfer when $\zeta = 0$, and should fit on the line

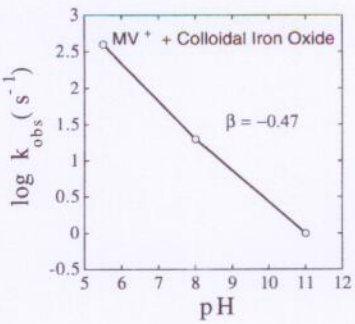

Figure 12.13. Transfer coefficient for electron transfer to iron oxide by methyl viologen radical cations at infinite ionic strength using limiting values at pH 5 and 11 and at the pzc of pH 8.3. Fit to Eq. (12.42), assuming $\zeta = 0$, at infinite ionic strength. Adapted from ref. 23.

represented by the reduced form of Eq. (12.34), namely,

$$\log k_{et} = \log k_{pzc} - \beta(\mathrm{pH} - \mathrm{pzc}) \tag{12.42}$$

Using the two infinite ionic strength rate constants gives a value of $\beta = 0.47$. This value is the 'true' transfer coefficient for oxidation of methyl viologen radical cations by colloidal iron oxide. Note that at low ionic strength, an experimental analysis of the transfer kinetics over only one or two pH units could easily have led to the conclusion that the radical is either negatively charged or positively charged.

The identification of the zeta potential with the potential at the plane of electron transfer has a further use if, a priori, the transfer coefficient is known. The existence of maxima or minima in the rate of an interfacial charge transfer reaction can then be predicted from Eq. (12.34) following differentiation:

$$\frac{\partial \log k_{et}}{\partial \mathrm{pH}} = 0 = -\beta\,\mathrm{pH} - \frac{\partial \zeta}{\partial \mathrm{pH}} \frac{(\beta + z_R)F}{2.303RT} \tag{12.43}$$

Hence at the maximum or minimum,

$$0.0592 \frac{\beta}{\beta + z_R} \mathrm{pH} = \frac{-\partial \zeta}{\partial \mathrm{pH}} \tag{12.44}$$

and the slope of the zeta vs. pH curve determines the value of the pH at which a maximum or minimum in the rate of electron transfer occurs. Thus proper characterization of the colloid double layer is essential when attempting to optimize electron transfer.

Another interesting case is the study by Moser et al. of the reduction of a cobaltacenium dicarboxylate anion as a function of pH using photoexcited colloidal TiO_2 [28]. They observed a decrease in the rate with increasing pH, contrary to earlier results with methyl viologen and proposed that the redox active anion was involved in an acid-base equilibrium with a dianion, which was in turn postulated to be electrochemically inert. The effective concentration of the electroactive acceptor then decreased with increasing pH, and this was used to explain the observed

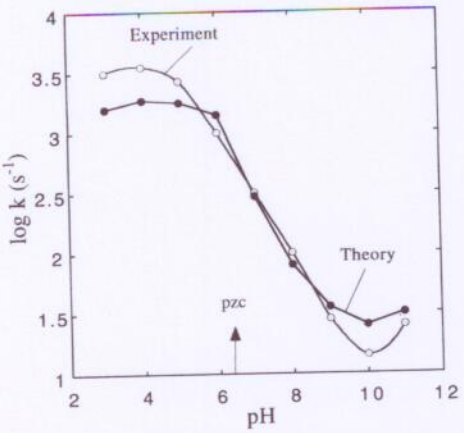

Figure 12.14. Observed dependence of the rate of electron transfer from photoexcited colloidal TiO_2 to cobaltacenium dicarboxylate anions on pH and the calculated rates relative to the pzc predicted using the zeta potential data of Wiese and Healy and assuming $z = -1$, and an ionic strength of 1 mM. The entire pH dependence including the slope and absolute value at the minimum near pH 11 is predicted from Eq. (12.35) with $\beta = 0.5$, $z = -1$.

decreased rate of electron transfer. However, a simpler explanation is that the increasingly negative zeta potential at high pH is responsible for the rate decrease. In Figure 12.14, we have fitted their data to Eq. (12.35). This equation accurately predicts both the decrease and the minimum at pH 10.5, and the eventual upturn in the rate, which is not easily explained via the dissociation mechanism.

12.4.4 Non-Nernstian Behavior

Equation 2, the Nernst equation, is clearly fundamental to the interpretation of all the data presented so far, yet we cannot directly measure ψ_o, only a potential at the plane of shear. Charge titration curves obtained from metal oxide suspensions are dramatically different to those obtained on silver halides or mercury, and suggest very large inner layer capacitances [10, 11, 13], implying that the Helmholtz region around metal oxides is a vastly different environment to that around mercury. It now seems clear that for any insulating or semiconducting surface, where the lattice ions themselves are not the potential determining ones, as is the case for AgI where Ag^+ and I^- determine the surface potential, an alternative formulation for the surface charging mechanism is required. These are termed "ionizable surface group models". For oxides, the surface is considered to act as an amphoteric acid and base with fundamental surface reactions of the form

$$AH_2^+ \Longrightarrow AH + H^+ \tag{12.45}$$

$$AH \Longrightarrow A^- + H^+ \tag{12.46}$$

determining the surface charge. Here A denotes the surface group on the particle. Each reaction has an associated equilibrium or surface acidity constant, K_{a1} and K_{a2}. Analysis of such surface ionization models suggests that Nernstian behaviour is a limiting form for most surfaces. Healy and White [11] show that deviations from Nernstian behaviour can be characterised by pK, where $pK = pK_{a1} - pK_{a2}$. It defines the difference in acidity of the surface groups. The values can only be determined experimentally, and the resulting equations for the surface potential can only be solved numerically or graphically [10].

The effects of non-Nernstian behaviour on the kinetics of electron transfer have not been examined to date. In principle, if $d\psi_o/dpH < 59$ mV/pH, then the difference must appear as a potential difference within the oxide, but this will only be established by slow proton diffusion through the solid [35]. The two metal oxides for which data are available, TiO_2 and Fe_2O_3, are both reasonably Nernstian, and the fits to the kinetic data are noticeably inferior if less than Nernstian response of ψ_o to pH is assumed in the calculations. Furthermore, flat band measurements on ZnO and TiO_2 prove unequivocally that the bulk energy levels within the metal oxides are shifted by -59 mV/pH change in solution [36, 37]. It is worthwhile noting that ionizable surface group models consistently require large inner layer capacitances (>100 μF cm^{-2}) to reconcile charge titration and electrokinetic data, and the data for electron transfer from viologen radicals to iron oxide can likewise only be reconciled using a large Stern layer capacitance of 450μF cm^{-2}. So both the e.t. kinetics and charge titration/electrophoresis data indicate that the Helmholtz region of metal oxides is very different to the mercury–water interface.

12.4.5 Extensions to Other Systems

There is a paucity of clear data on e.t. to metal sulphides, or other chalcogenides (MX), as a function of pH or [H_2X]. In the case of metal halides, Hoffman and Billings showed that the reduction overpotential of an AgBr electrode varied with pBr [38]. Morrison has reviewed the data for CdS and other sulphide systems, but the conclusions are unclear [37]. Since many workers do not control [H_2S] of the sols after preparation, surface potential control is not possible. Ginley and Butler demonstrated by charge titration that the Fermi level in a CdS electrode is controlled by pH and [HS^-] [39]. van Leeuwen and Lyklema have reported on AgI electrode measurements in which they examine both ion adsorption and electron transfer; their review also discusses processes such as double layer relaxation [40].

12.5 The Effect of Zeta on Radical Scavenging Yields

The viologen radical does not undergo recombination at a perceptible rate, and so it is possible to examine the effect of the double layer upon mass transfer and activation controlled reactions with this radical using quite simple modifications of the Tafel and Smoluchowski equations. In general however, excited species generated

by either photolysis or radiolysis undergo various deactivation pathways in addition to reaction with substrates such as colloidal particles. In the case of photolysis, these are usually first-order radiative or nonradiative energy losses, and these are readily incorporated into the equations above. A more common situation in radiolysis is that the radical undergoes self-reaction, i.e. second order loss. Furthermore a number of radicals have pK_a's in the common range of solution acidities. The charged, anionic form will interact with the colloid double layer. Rao and Hayon [41] have made extensive measurements of radical pK_a's by spectrophotometric means, and Henglein and colleagues have measured many radical pK_a values by pulse radiolysis polarography [42]. The radical anion is a better reductant than the neutral, 'acidic' form [41], and often recombination of the charged anionic form is slower than recombination of the neutral radical. Trying to unravel these various effects is an arduous one. In the following, we describe some model calculations on how the double layer parameters control scavenging yields of radicals by colloidal iron oxide particles. We summarize a typical scenario in Figure 12.15, where we show how the radical speciation and particle charge might change with pH.

The scavenging of the radicals under steady state conditions will depend upon both the pK_a of the radical, the pzc of the oxide and whether the reaction is diffusion controlled or activation controlled. For activation controlled processes, it is necessary to know k_{pzc}, the intrinsic rate of transfer at the point of zero charge, for both the acid and base forms of the radical. For activation controlled electron transfer, double layer corrections are also required for neutral radicals. This follows from Eq. (12.34) with $z_R = 0$.

For mass transfer limited reactions of radicals with colloid particles, the position is slightly simpler. Given a well defined acidity constant K_a for the dissociation,

$$RH \Longleftrightarrow R^- + H^+ \tag{12.47}$$

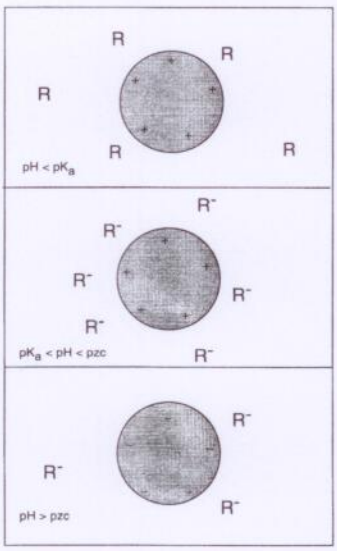

Figure 12.15. Diagram illustrating the changing speciation of radicals and charge around a metal oxide colloid particle. (Top): $pH < pK_a$ and all radicals neutral and oxide positively charged. (Middle): pH raised until $pzc > pH > pK_a$. Radical anion now predominates and local concentration around oxide particles is enhanced. (Bottom): At higher pH, the oxide particle becomes negatively charged and radical anions are depleted near particle surface.

where RH and R^- are the acid and basic forms of the radical respectively, the fraction of radicals initially present in the protonated form is $\alpha = [RH]/[R]_t = 1/(1 + K_a/[H^+])$, and those in the deprotonated form is $(1 - \alpha)$, where the total radical concentration is $[R]_t$. The rate of disappearance at any pH is then due to recombination of both protonated and deprotonated radicals as well as to colloid encounters by both charged and uncharged radicals.

$$d[R]_t/dt = G(R)D - k_{diff}[R]_t[colloid] - k_{field}(1 - \alpha)[R]_t[colloid] - 2\alpha^2 k_1[R]_t^2 - 2\alpha(1 - \alpha)k_2[R]_t^2 - 2(1 - \alpha)^2 k_3[R]_t^2 \quad (12.48)$$

where k_{field} is the encounter rate constant using Eq. (12.32), k_{diff} is the field-free diffusion controlled rate constant given by Eq. (12.30), while k_1, k_2 and k_3 are the recombination rate constants for radical–radical deactivation, and G(R)D is the production rate of the radical, which for radiolytically generated radicals, is the dose rate, D, times the G value for the species R. Using the steady state approximation, Eq. (12.48) becomes quadratic in $[R]_t$ and the steady state radical concentration is readily found to be

$$[R]_{ss} = \frac{-K_d + (K_d^2 - 4K_r G(R)D)^{1/2}}{2K_r} \quad (12.49)$$

where

$$K_r = 2\alpha^2 k_1 + 2(1 - \alpha)k_2 + 2(1 - \alpha)^2 k_3 \quad (12.50)$$

and

$$K_d = \{(1 - \alpha)k_{diff} + k_{field}\,\alpha\}[colloid]. \quad (12.51)$$

The value $[R]_{ss}$ can then be inserted into Eq. (12.49) to determine the fraction disappearing by recombination and the fraction scavenged by the colloid. The scavenging efficiency, λ, is then defined as

$$\lambda = \frac{K_d}{K_d + K_r[R]_{ss}} \quad (12.52)$$

To get a feel for the size of the double layer effects, we have taken the formic acid radical with a pK_a of 3.4 as the reductant, and colloidal iron oxide as the colloid. In Figure 12.16, the speciation and colloid charge as a function of pH are shown. In Figure 12.17, λ is plotted as a function of the colloid concentration for a number of pH's. In the calculations, it was assumed that $a = 20$Å and $k_1 = k_2 = k_3 = 1 \times 10^{10}\ M^{-1}s^{-1}$. As is very clear, the scavenging shows a strong pH dependence, and a maximum occurs at a pH where the radical is deprotonated, but the oxide is still positively charged. As the pH is increased through the pzc, the efficiency decreases dramatically, because both the sol and the radical become negatively charged (see Figure 12.18). Clearly, a primary prerequisite for achieving high effi-

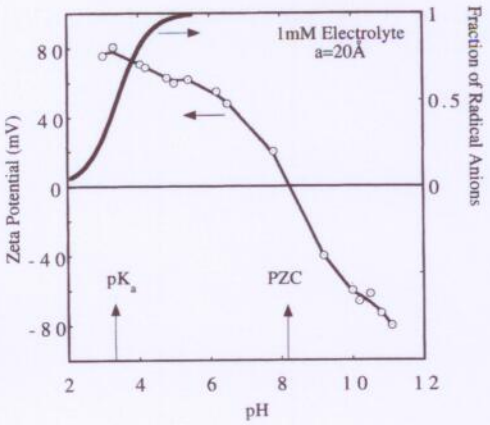

Figure 12.16. The measured zeta potential for nanosized iron oxide particles vs pH at 1 mM electrolyte and the relative population of radicals and radical anions assuming a pK_a of 3.4.

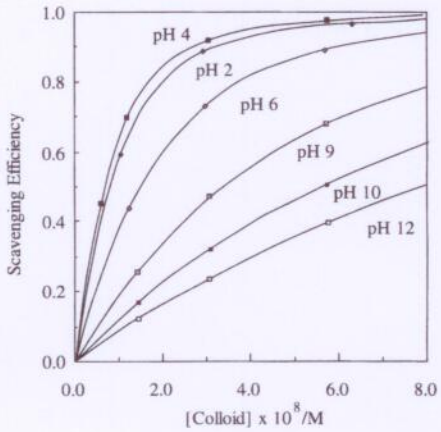

Figure 12.17. The radical scavenging efficiency of colloidal iron oxide as a function of colloid concentration and pH using parameters in Figure 12.16.

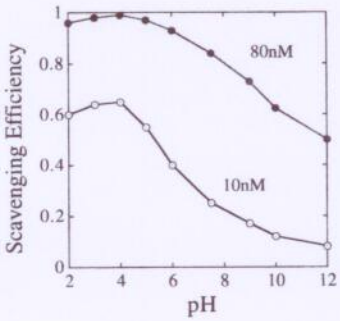

Figure 12.18. The radical scavenging efficiency of colloidal iron oxide as a function of pH at two colloid concentrations. The efficiency peaks at a pH between the pK_a and pzc due to enhanced mass transfer to the colloid particles.

ciency is that pzc > pK_a. However, even if the pzc < pK_a, recombination of the radical anion is often slower than for the neutral form, so higher yields may still be found even with electrostatic repulsion. Thus when a redox reaction is under diffusion control, the double layer may exert a significant effect on the rate of reaction and the efficiency of radical scavenging.

12.6 Colloid Nucleation and Nanoparticle Stability

In this final section, we address briefly the role of stabilizers for nanoparticles. Even colloidal metals which have high Hamaker constants and which should be susceptible to coagulation can be made as sols with quite low zeta potentials that are stable for months at a time. What does the double layer tell us about preparing nanosized particles in water? For the case of low potentials, and small overlap between double layers, the results are quite unexpected. The electrostatic repulsive energy for two spheres of radius a, with low surface potential ψ_o, approaching each other in a medium of Debye length κ^{-1} is given by:

$$V_{rep}(kT) = 4\pi\varepsilon_r\varepsilon_o\psi_o{}^2a^2/r \exp(-\kappa a(r/a - 2)) \tag{12.53}$$

The nonretarded van der Waals attractive energy between particles of radius a is given by

$$V_{att}(kT) = -A/6\{2a^2/(r^2 - 4a^2) + 2a^2/r^2 + \ln(1 - 2a^2/r^2)\} \tag{12.54}$$

with $r > 2a$, the centre-to-centre distance. According to DLVO theory it is the sum of the two energies that determines particle stability. The usual criterion are that a barrier of 15–20kT is sufficient to ensure colloid stability. These two functions are plotted in Figures 12.19 and 12.20 as a function of the particle surface separation and for various particle sizes [43]. It is clear from Eqs. (12.53) and (12.54), that the interaction energy increases with particle radius, a, for both the attractive and repulsive energy. As a consequence, we can see in Figure 12.21 that the barrier height to colloid stability at fixed ψ_o increases as the particle size increases. Consequently,

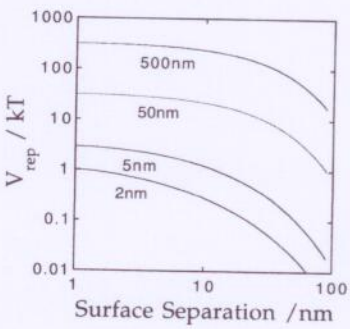

Figure 12.19. The calculated repulsive interaction energy between colloid particles calculated using Eq. (12.53), as a function of the particle separation for a range of diameters from the nanometre to micrometre size regime. Parameters used: $\psi_o = 25$ mV, $\kappa^{-1} = 100$Å.

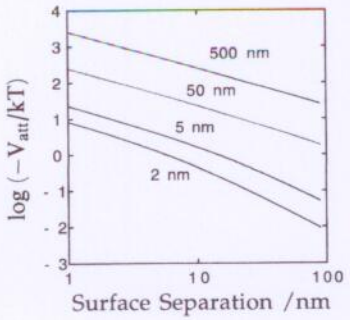

Figure 12.20. The calculated nonretarded van der Waals interaction energy between colloid particles calculated using Eq. (12.54), as a function of the particle separation for a range of diameters from the nanometre to micrometre size regime. Parameters used: $A = 6 \times 10^{-20}$ J.

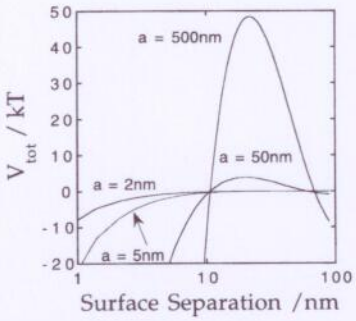

Figure 12.21. The total interaction energy due to both repulsive and attractive forces. Conditions as per Figures 12.19 and 12.20. Critical to nanoparticle nucleation and stabilization in solution is that the repulsive energy is smaller for small particles so a larger zeta potential is required for colloidal stability, but the primary minimum created by attractive dispersion interactions is likewise smaller, so that stabilization by adsorbed polymers, surfactants or chemisorbed complexing agents, such as thiols or small carboxylic acids, is much more efficacious than for larger colloid particles.

there is an automatic tendency for coagulation of particles to slow down as coagulation proceeds. This factor may often determine the final particle size distribution following nucleation. But the primary minimum associated with particle coalescence also becomes deeper as the particle size increases. If two particles > 10 nm in size coalesce in solution, they will not be able to separate again since their thermal energy will be insufficient to allow them out of the primary minimum. Conversely, nanosized particles will peptize relatively easily. It is important to recognize that rapid peptization is essential. An agglomerate of small particles will behave in van der Waals terms like a larger particle and the van der Waals interaction energy with other unpeptized particles will gradually increase if agglomeration is allowed to continue. Provided nanoparticles peptize quickly, the van der Waals potential well around the temporary agglomerate will not have time to deepen further via aggregate–colloid encounters.

It is clear from these figures that only small molecules should be necessary to prevent coalescence and particle coagulation of nanoparticles. Chemisorbed mole-

cules provide a steric barrier, and for particles <100Å in diameter, this will be sufficient to offset the van der Waals interactions. However, ψ_o should be large to prevent the formation of loose agglomerates. Thus, small stabilizers can be remarkably efficacious in stabilizing nanosized colloid particles.

12.6.1 Some Unresolved Aspects of Colloid Redox Chemistry

The aim of this chapter has been to show how the measured properties of powders and suspensions in liquids are important not just from the thermodynamic or colloid stability viewpoint. The equations describing the electrical double layer around particles also govern the kinetic response to redox disequilibria in solution, and rates of electron transfer can be controlled and optimized once the various factors are understood. Disappointingly, there have been few studies to elucidate how specific adsorption at a colloid surface affects electron transfer, yet most nanosized particles can only be prepared in the presence of strong growth inhibitors such as polyelectrolytes which strongly adsorb to the particle surface. Darwent's work on the effects of sulfate adsorption remains an exception [29], and the PhD work by

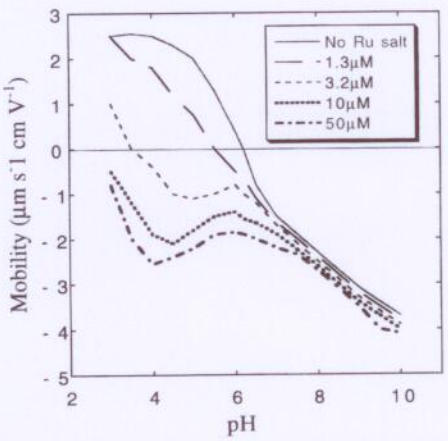

Figure 12.22. Effect of pH on the electrophoretic mobility of colloidal TiO_2 in the presence of tris(2,2′-bipyridine-4,4′-dicarboxylic acid) ruthenium (II). Specific adsorption occurs below the pzc of 6.1. If adsorption occurs at the outer Helmholtz plane (close to the shear plane), then there will be a dramatic increase in the overpotential for electron injection into the titania colloid, which depends exponentially on the potential across the Helmholtz layer. If we assume that ψ_o is constant for a particular pH value then we predict that the rate of electron injection should be enhanced through Eq. (12.34) by an amount $\exp(\beta F(\psi_o - \zeta))/RT$. The negative charge on the adsorbed sensitizer not only aids adsorption to the positively charged colloid particles, but simultaneously accelerates injection by creation of an increased Helmholtz potential difference. The degree of enhancement is critically determined by the location of the planes of dye adsorption and electron transfer. Adapted from ref. 45.

Kleijn on the effects of viologen adsorption on RuO_2 electrokinetics is another [44]. These adsorption effects may also play a prominent role in systems such as dye sensitized photoelectron transfer, which has recently been demonstrated as a viable basis for charge separation in solar energy conversion [6]. In the so-called Grätzel cell, high surface area electrodes are synthesized by sintering metal oxide colloid films. The sensitizer is adsorbed primarily electrostatically, but the act of chemisorption modifies the potential distribution at the surface, and this may act to augment or hinder the electron injection rates following illumination. That such effects will be important is immediately apparent from the zeta potential data for titanium dioxide colloids in the presence of the anionic ruthenium dye shown in Figure 12.22 [45]. In this case, since the photoelectron transfer is anodic, the adsorption of the negatively charged dye onto the positively charged metal oxide particles could be beneficial. The zeta potential becomes more negative, but we assume that at any pH, the actual surface potential is fixed by Eq. (12.2), so the adsorption must introduce a large electric field across the Helmholtz layer, driving electron transfer into the particle. This synergistic effect may enhance the rates of e.t. by a factor of 10–100, based on the data in Figure 12.22.

Studies on the effects of complexing agents on rates of electron transfer could well assist in the formulation of additives to improve industrially important redox reactions such as rust removal. The role of extraneous ligands on electron transfer to iron oxide are still speculative. For example, would o-phenanthroline, a potent, neutral complexing agent for Fe(II) slow down e.t. from viologen radicals to colloidal iron oxide by specific adsorption to the surface, thus blocking viologen approach? Or would it conversely aid e.t. by prebinding to selected Fe(III) surface sites, accelerating the actual rate of e.t. to these specific, activated sites? Or would it simply accelerate the rate of Fe(II) desorption following reduction, thereby exposing fresh Fe(III) surface sites more quickly and by this mechanism accelerate particle dissolution? To date only steady state dissolution data are available to help answer these detailed mechanistic questions [46].

What at least should be clear is that simple electron transfer is governed by the overall electrical potential distribution at the colloid surface, with the zeta potential governing the local surface concentration of charged reactants, and the difference $(\psi_o - \zeta)$ acting as the overpotential for actual transfer from solution to surface. The relative rates at different pH's can be accurately predicted when no specific adsorption occurs if ζ potentials are determined. If the actual data are to be believed, then the plane of electron transfer lies slightly closer to the surface than the plane of shear, which determines the electrokinetic or zeta potential, a conclusion consistent with modern views about the electrical double layer. Frumkin, the discoverer of the diffuse layer effect in electrode kinetics, would have been happy [17, 18], to see the same effects so prominent in colloid redox kinetics too.

In the case of mass transfer limited reactions, there are no data to indicate whether the dramatic effects predicted from the calculations in Figures 12.5 and 12.6 really occur. Such drastic retardation must have important implications for enzyme catayzed reactions as well as colloid redox chemistry. For example, one might expect that the reaction

$$2Fe(CN)_6^{4-} + MnO_2 + 4H^+ \Longrightarrow Mn^{2+} + 2Fe(CN)_6^{3-} + 2H_2O \quad (12.55)$$

would be close to mass transfer limited given the strong $\Delta E^o = 1.2V$ for reaction. Yet 250Å MnO_2 sols have zeta potentials of -50 mV at pH 6, so the rate of e.t. is predicted to lie at 10^8 $M^{-1}s^{-1}$, not 10^{11} $M^{-1}s^{-1}$. Likewise reactions such as the disproportionation of superoxide anions by superoxide dismutase, which has a negative mobility at physiological pH, would be hindered by slow migration of the substrate to enzyme active sites at low ionic strength.

In this article, we have not discussed the electrical double layer within colloid particles since this remains a basic unknown in colloid science. Microwave conductivity offers the prospect of determining the concentrations of carriers, at least in nonaqueous systems, but there are again no data except for flat band potentials measured on sintered nanocrystalline electrodes from which to evaluate donor densities, trap energies or internal space charge potentials [6].

Fundamental to the understanding of charge injection into insulating materials is the concept that the potential determining ions regulate the surface potential independently of the charge injected through redox reactions. This can be justified on the basis of the small space charge capacitance compared with the solution phase Helmholtz capacitance. Consequently for a fixed chemical potential of the proton in the bulk solution, the surface potential is fixed, and charge transfer into or out of the particle must be accompanied by proton adsorption or desorption [24, 25]. Because of the facility of these reactions, one can normally assume that an insulating particle retains a constant surface potential during a redox reaction, though obviously after extensive reaction, the chemical potential of the proton within the solid or in the bulk may have changed.

A final, interesting question which appears never to have been systematically investigated is whether the van der Waals forces at the surface have any effect on the rate of electron transfer to and from solution. In principle, the mass transfer rate constant for *all* electroactive species will be enhanced at small separations (< 10nm) by dispersion forces, since the molar refractive index of the electroactive species differs from the average refractive index of the medium. The dispersion interaction will not be as important as it is for colloid–colloid interactions because of the small radius of the electroactive species – see Figure 20, but it may still be significant enough to cause perceptible changes in the observed rates of mass transfer to charged surfaces. Whether this effect can be harnessed as a means to further optimize e.t. is still to be determined. Thus, though we have set out to show that the theoretical foundations linking colloid chemistry and electrochemistry have been further bolstered and consolidated through the research on colloid redox chemistry over the last decade or two, many basic questions remain unresolved.

Acknowledgements

This work was supported by an ARC Research Grant. The author is also grateful for the support of the Advanced Mineral Products Research Centre.

References

[1] E. J. Verwey, J. T. Overbeek, *Theory of the Stability of Lyophobic Colloids*, Elsevier, Amsterdam **1948**.
[2] T. H. James, *Theory of the Photographic Process*, 4th edn., MacMillan, London **1977**.
[3] M. A. Blesa, E. B. Borghi, A. J. G. Maroto, A. E. Reggazoni, *J. Coll. Interface Sci.* **1984**, *98*, 295.
[4] D. Bradbury, in: *Water Chemistry of Nuclear Reactor Systems*, British Nuclear Energy Society, London **1978**, p. 373.
[5] J. D. Hem, *Chem. Geol.* **1978**, *21*, 199.
[6] B. O'Regan, J. Moser, M. Anderson, M. Grätzel, *J. Phys. Chem.* **1990**, *94*, 8720.
[7] O. Micic, D. Meisel, in: *Homogeneous and Heterogeneous Photocatalysis* (Eds.: E. Pelizzetti, N. Serpone), NATO ASI Series C174, Reidel, Dordrecht, **1986**.
[8] For example, see F. C. Tye, *Electrochimica Acta* **1985**, *30*, 17; **1974**, *21*, 415.
[9] R. J. Hunter, *Zeta Potential in Colloid Science*, Academic Press, London **1981**.
[10] T. W. Healy, L. R. White, *Adv. Colloid Interface Science* **1978**, *9*, 303.
[11] R. O. James, G. A. Parks, in: *Surface and Colloid Science* (Ed.: E. Matijevic), Vol. 12, Plenum Press, New York **1982**.
[12] G. A. Parks, *Chem. Rev.* **1965**, *65*, 177.
[13] R. J. Hunter, *Foundations of Colloid Science*, Vol. 1, Oxford University Press, Oxford **1989**.
[14] J. H. Fendler, F. C. Meldrum, *Adv. Mater.* **1995**, *7*, 607.
[15] J. H. Fendler, in: *Nanoparticles in Solids and Solutions* (Eds.: J. H. Fendler, I. Dekany), NATO ASI Series, Kluwer, Dordrecht **1996**.
[16] (a) C. E. Zobell, *Bull. Am. Chem. Assoc. Petrol. Geol.*, **1946**, *30*, 477; (b) R. M. Garrels, C. L. Christ, *Solutions, Minerals and Equilibrium*, Jones and Bartlett, Boston **1990**.
[17] R. Parsons, *Modern Aspects of Electrochemistry* **1954**, *1*, 103.
[18] P. Delahay, *Double Layer and Electrode Kinetics*, Wiley, New York **1965**.
[19] H. Ohshima, T. W. Healy, L. R. White, *J. Colloid Interface Sci.* **1982**, *90*, 17.
[20] S. Rice, in: *Comprehensive Chemical Kinetics* (Eds.: C. Bamford, C. Tipper, R. Compton), Vol. 5, Elsevier, Amsterdam **1985**.
[21] A. Henglein, *Ber. Bunsenges. Phys. Chem.* **1982**, *86*, 241.
[22] (a) J. Albery, *Electrode Kinetics*, Clarendon Press, Oxford **1975**; (b) A. J. Bard, L. R Faulkner, *Electrochemical Methods*, Wiley, New York **1980**.
[23] P. Mulvaney, Ph.D. Thesis, University of Melbourne **1988**.
[24] P. Mulvaney, V. Swayambunathan, F. Grieser, D. Meisel, *J. Phys. Chem.* **1988**, *92*, 6732.
[25] (a) P. Mulvaney, V. Swayambunathan, F. Grieser, D. Meisel, *Langmuir* **1990**, *6*, 555; (b) P. Mulvaney, F. Grieser, D. Meisel, in: *Proceedings of the 9th International Congress of Radiation Research*, Toronto, Academic Press, New York **1991**.
[26] M. Grätzel, A. J. Frank, *J. Phys. Chem.* **1982**, *86*, 2964.
[27] D. Duonghong, J. Ramsden, M. Grätzel, *J. Am. Chem. Soc.* **1982**, *104*, 2977.
[28] U. Kölle, J. Moser, M. Grätzel, *Inorg. Chem.* **1985**, *24*, 2253.
[29] J. R. Darwent, A. Lepre, *J. C. S. Faraday Trans.* 2 **1986**, *82*, 2323.
[30] G. T. Brown, J. R. Darwent, *Chem. Comm.* **1985**, 98.
[31] G. T. Brown, J. R Darwent, P. D. I. Fletcher, *J. Am. Chem. Soc.* **1985**, *107*, 6446.
[32] I. Willner, J.-M. Yang, C. Laane, J. W. Otvos, M. Calvin, *J. Phys. Chem.* **1981**, *85*, 3277.
[33] (a) D. W. Bahnemann, C. Kormann, M. R. Hoffmann, *J. Phys. Chem.* **1987**, *91*, 3789; (b) C. Kormann, D. W. Bahnemann, M. R. Hoffmann, *J. Phys. Chem.* **1988**, *92*, 5196.
[34] G. R. Wiese, T. W. Healy, *J. Colloid Interface Sci.* **1975**, *51*, 427.
[35] M. A. Butler, *J. Electrochem Soc.* **1979**, *126*, 338.
[36] M. A. Butler, D. S. Ginley, *J. Electrochem Soc.* **1978**, *125*, 228.
[37] S. R. Morrison, *Electrochemistry at Semiconductor and Oxidized Metal Eectrodes*, Plenum Press, New York **1980**.
[38] A. Hoffman, B. Billings, *J. Electroanal. Chem.* **1977**, *77*, 97.
[39] D. S. Ginley, M. A. Butler, *J. Electrochem Soc.* **1978**, *125*, 1968.

[40] H. P. van Leeuwen, J. Lyklema, in: *Modern Aspects of Electrochemistry*, Vol. 17 (Eds.: J. O'M. Bockris, B. E. Conway, R. E. White), Plenum Press, New York **1986**.
[41] P. Rao, E. Hayon, *J. Am. Chem. Soc.* **1974**, *96*, 1287.
[42] A. Henglein, *Electroanal. Chem.* **1976**, *9*, 163.
[43] G. R. Wiese, T. W. Healy, *Trans. Fara. Soc.*, **1970**, *66*, 490.
[44] M. Kleijn, Ph.D. Thesis, University of Wageningen **1987**.
[45] D. N. Furlong, D. Wells, W. H. F. Sasse, *J. Phys. Chem.* **1986**, *90*, 1106.
[46] V. I. E. Bruyere, M. A. Blesa, *J. Electroanal. Chem.* **1985**, *182*, 141.